A Unified Bayesian Approach to Extract Network-Based Functional Differences from a Heterogeneous Patient Cohort

Archana Venkataraman[1], Nicholas Wymbs[2,3], Mary Beth Nebel[2,3], and Stewart Mostofsky[2,3,4]

[1]Department of Electrical & Computer Engineering, Johns Hopkins University, USA
[2]Center for Neurodevelopmental Medicine & Research, Kennedy Krieger Institute, Johns Hopkins Scool of Medicine, USA
[3]Department of Neurology, Johns Hopkins School of Medicine, USA
[4]Department of Pediatrics, Johns Hopkins School of Medicine, USA

Abstract. We present a generative Bayesian framework that automatically extracts the hubs of altered functional connectivity between a neurotypical and a patient group, while simultaneously incorporating an observed clinical severity measure for each patient. The key to our framework is the latent or hidden organization in the brain that we cannot directly access. Instead, we observe noisy measurements of the latent structure through functional connectivity data. We derive a variational EM algorithm to infer both the latent network topology and the unknown model parameters. We demonstrate the robustness and clinical relevance of our model on a population study of autism acquired at the Kennedy Krieger Institute in Baltimore, MD. Our model results implicate a more diverse pattern of functional differences than two baseline techniques, which do not incorporate patient heterogeneity.

1 Introduction

Functional connectomics explores the intrinsic organization of the brain via the underlying assumption that two regions, which reliably co-activate are more likely to participate in the same neural processes than two uncorrelated or anti-correlated regions [1]. It has become ubiquitous in the study of neurological disorders, such as schizophrenia and autism. From a practical standpoint, these functional relationships are typically evaluated in resting-state fMRI (rsfMRI), which does not require patients to complete challenging experimental paradigms. Neuroscientifically, group-level changes in the functional architecture of the brain are treated as biomarkers of a particular neurological condition.

State-of-the-art methods follow a two-step procedure of first fitting a connection- or graph-based model and then identifying group differences. Unfortunately, connection-based effects [2] are difficult to interpret and nearly impossible to verify through direct stimulation. While large-scale graph properties, such as modularity [3] and small-worldness [4], mitigate these limitations, are markedly

removed from the original network and rarely illuminate a concrete etiological mechanism. Additionally, most studies implicitly treat the patient group as homogeneous, for example, by conducting a statistical evaluation that differentiates patients from controls. This simplification has likely contributed to the lack of reproducible rsfMRI findings in the clinical literature [5].

This paper tackles a fundamental yet overlooked question in the study of functional connectomics: how do we identify the altered functional pathways given a heterogeneous patient cohort? Going one step beyond conventional graph analytics, we will characterize *the full network topology*, i.e., the entire collection of nodes (brain regions) and edges (functional connections) associated with the affected subnetwork. Our framework is based on two guiding principles: (1) complex neurological disorders reflect a distributed but interrelated network of functional impairments, (2) the influence of this affected subnetwork is moderated by the observed clinical severity. Hence, rather than dismissing or regressing out the clinical scores, these measures will crucially guide our network estimation procedures. We draw from the Bayesian model of [6]; however, our novel data likelihood reflects the patient-specific contributions of two functional templates.

We evaluate our model on a population study of Autism Spectrum Disorder (ASD). ASD is characterized by impaired social-communicative skill and awareness across multiple sensory domains, coupled with restricted/repetitive behaviors. Despite ongoing efforts, the complex and heterogeneous presentation of ASD has impeded the discovery of robust neuroimaging biomarkers for the disorder. Functional connectomics has largely implicated the default mode [7] and large-scale network measures [2]. However, these approaches blur information across regions and connections, so it is unclear what neural processes are being impacted. In contrast, our mathematical framework will automatically infer the altered functional pathways, as informed by autism severity.

2 Generative Model of Abnormal Communities

We hypothesize that a given neurological disorder reflects *coordinated disruptions* in the brain. Although we cannot specify *a priori* where these disruptions will occur, we assume that the affected regions will communicate differently with other parts of the brain than if the disorder were not present. In the functional connectomics realm, our assumption can be modeled by region hubs, which exhibit a large number of altered functional connections, as compared to the neurotypical cohort. Below, we refer to these region hubs as *disease foci*; the altered connectivity pattern is termed the *canonical network*.

Following the methodology of [6], we define latent functional connectivity templates F_{ij} and $\bar{F}_{ij}$, which capture the neural synchrony between region i and region j in the neurotypical (i.e., control) and clinical populations, respectively. Empirically, we find that three states: low ($F_{ij} = 0$), medium ($F_{ij} = 1$), and high ($F_{ij} = 2$), best capture the dynamic range and variability of our data. The rsfMRI correlation B_{ij}^l for control subject l is a noisy observation of the latent template F_{ij}. However, the rsfMRI correlations $\{\bar{B}_{ij}^m\}$ for patient m are drawn

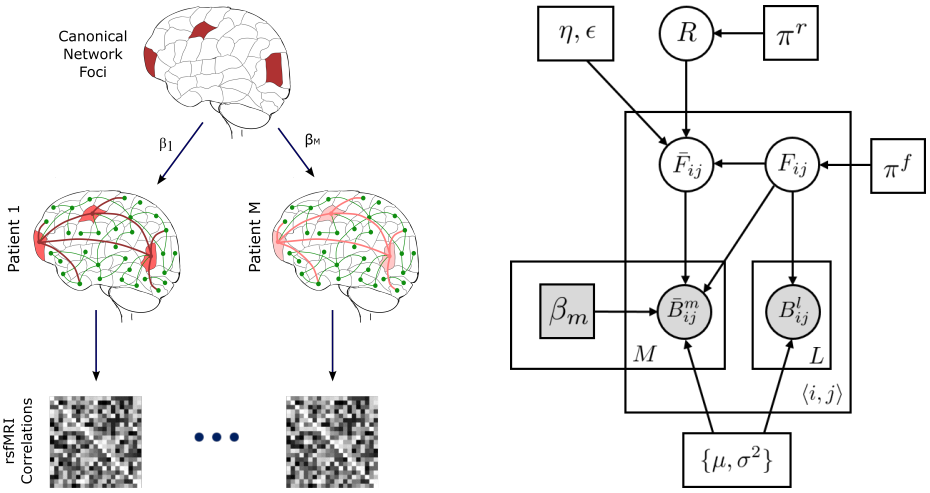

Fig. 1. Hierarchical network model. **Left:** Conceptual diagram of behavioral influence. Red regions correspond to the disease foci, and red edges specify the canonical functional network. Green edges are normal (i.e., healthy) connections. The canonical network contribution for each patient m is specified by the clinical severity, $\beta_m \in [0, 1]$. Here, $\beta_1 > \beta_M$, as indicated by the darker edges. **Right:** Graphical model representation. The label R_i indicates whether region i is healthy or abnormal. The neurotypical template $\{F_{ij}\}$ provides a baseline functional architecture for the brain, whereas the clinical template $\{\bar{F}_{ij}\}$ describes the canonical network organization. The patient rsfMRI correlations $\{\bar{B}^m_{ij}\}$ are generated according to the clinical scores $\{\beta_m\}$.

from either latent template in proportion to the observed clinical severity $\beta_m \in [0, 1]$. Fig. 1 outlines the full generative process.

Our discrete representation of latent functional connectivity is a notable departure from conventional analysis. Essentially, we assume that the rsfMRI correlations fall into one of three general categories, and that differences in the *bin assignments* are the relevant markers of a disorder. The beauty of our framework is that we isolate the disorder-induced effects in the latent structure, while accommodating noise and subject variability via the data likelihood.

Disease Foci: The binary variable R_i indicates whether region i is healthy ($R_i = 0$), or whether it is a disease foci ($R_i = 1$). We assume an *i.i.d.* Bernoulli prior: $P(R_i = 1; \pi^r) = \pi^r$. The unknown parameter π^r is shared across regions.

Latent Network Topology: The latent functional connectivity F_{ij} denotes the co-activation between regions i and j in the neurotypical template. Once again, F_{ij} is modeled as a tri-state random variable with an *i.i.d.* multinomial prior across all pairwise connections: $P(F_{ij} = s; \pi^f) = \pi^f_s$, $\forall s = 0, 1, 2$.

The clinical template $\bar{F}_{ij}$ depends on both the neurotypical template F_{ij} and the region labels R. We define this variable via three simple rules: (1) a

connection between two disease foci is abnormal, (2) a connection between two healthy regions is normal, and (3) a connection between a healthy region and a disease foci is abnormal with unknown probability η. Ideally, $\bar{F}_{ij} = F_{ij}$ for healthy connections, and $\bar{F}_{ij} \neq F_{ij}$ for abnormal connections. However, to better accommodate noise, we allow the clinical template to deviate from these rules with probability ϵ. Mathematically, the conditional distribution is given by

$$P(F_{ij}|F_{ij}, R_i, R_j, \eta, \epsilon) = \begin{cases} \epsilon^{F_{ij}^{\mathrm{T}}\bar{F}_{ij}} \left(\frac{1-\epsilon}{2}\right)^{F_{ij}^{\mathrm{T}}\bar{F}_{ij}}, & R_i = R_j = 1, \\ (1-\epsilon)^{F_{ij}^{\mathrm{T}}\bar{F}_{ij}} \left(\frac{\epsilon}{2}\right)^{F_{ij}^{\mathrm{T}}\bar{F}_{ij}}, & R_i = R_j = 0, \\ \epsilon_1^{F_{ij}^{\mathrm{T}}\bar{F}_{ij}} \left(\frac{1-\epsilon_1}{2}\right)^{F_{ij}^{\mathrm{T}}\bar{F}_{ij}}, & R_i \neq R_j, \end{cases} \quad (1)$$

where $\epsilon_1 = \eta\epsilon + (1-\eta)(1-\epsilon)$ reflects the interaction between the edge density η and the latent noise ϵ when the region labels differ. For convenience, we have represented the neurotypical connectivity F_{ij} as a length-three binary indicator vector $[F_{ij0} \quad F_{ij1} \quad F_{ij2}]^{\mathrm{T}}$, and likewise for the clinical template.

Data Likelihood: The rsfMRI correlation B_{ij}^l for subject l is generated from a Gaussian distribution, with mean and variance controlled by the neurotypical functional template F_{ij}, i.e., $P(B_{ij}^l|F_{ij} = s; \{\mu, \sigma^2\}) = \mathcal{N}\left(B_{ij}^l; \mu_s, \sigma_s^2\right)$.

In contrast, the patient likelihood weighs the relative contributions of the clinical and neurotypical templates according to the observed severity score $\beta_m \in [0, 1]$. Effectively, the patient rsfMRI correlation $\bar{B}_{ij}^m$ is sampled from a conditional Gaussian mixture with *a priori* probabilities β_m and $1 - \beta_m$.

Using the binary indicator representation for F_{ij} and $\bar{F}_{ij}$, we have

$$P(\bar{B}_{ij}^m|F_{ij}, \bar{F}_{ij}; \beta_m, \{\mu, \sigma^2\}) = \beta_m \left[\prod_{s=0}^{2} \mathcal{N}\left(\bar{B}_{ij}^m; \mu_s, \sigma_s^2\right)^{\bar{F}_{ijs}}\right] + (1-\beta_m)\left[\prod_{s=0}^{2} \mathcal{N}\left(\bar{B}_{ij}^m; \mu_s, \sigma_s^2\right)^{F_{ijs}}\right]. \quad (2)$$

Intuitively, patients with larger β_m will more closely follow the clinical template than patients with smaller β_m. The patient-specific analysis in Eq. (2) distinguishes our model from conventional methods and from the prior work of [6].

Variational Inference: We introduce a set of auxiliary random variables $\{Z_{ij}^m\}$, which indicate whether the corresponding rsfMRI measure $\bar{B}_{ij}^m$ is drawn from the clinical ($Z_{ij}^m = 1$) or neurotypical ($Z_{ij}^m = 0$) Gaussian mixture. This strategy allows us to eliminate the sum in Eq. (2) by replacing the conditional density of $\bar{B}_{ij}^m$ with the following joint distribution over Z_{ij}^m and $\bar{B}_{ij}^m$:

$$P(Z_{ij}^m, \bar{B}_{ij}^m|F_{ij}, \bar{F}_{ij}; \beta_m, \{\mu, \sigma^2\}) = P(Z_{ij}^m; \beta_m) P(\bar{B}_{ij}^m|F_{ij}, \bar{F}_{ij}, Z_{ij}^m; \{\mu, \sigma^2\})$$

$$= \left[\beta_m \prod_{s=0}^{2} \mathcal{N}\left(\bar{B}_{ij}^m; \mu_s, \sigma_s^2\right)^{\bar{F}_{ijs}}\right]^{Z_{ij}^m} \left[(1-\beta_m) \prod_{s=0}^{2} \mathcal{N}\left(\bar{B}_{ij}^m; \mu_s, \sigma_s^2\right)^{F_{ijs}}\right]^{1-Z_{ij}^m} \quad (3)$$

We combine the above terms to obtain the joint density of latent and observed random variables. Let $\Theta = \{\pi^r, \pi^f, \eta, \epsilon, \mu, \sigma^2\}$ denote the collection of unknown but non-random parameters, and recall that the clinical scores β_m are given. The region labels $\{R_i\}$ induce a complex dependency across pairwise connections $\langle i, j \rangle$. Therefore, we leverage a Variational EM framework to derive the Maximum Likelihood (ML) solution to our model [8].

Our approximate posterior distribution assumes the following factorized form:

$$Q(R, F, \bar{F}, Z) = \prod_{i=1}^{N} q_i^r(R_i; \tilde{\alpha}_i) \prod_{\langle i,j, \rangle} q_{ij}^c(F_{ij}, \bar{F}_{ij}; \tilde{\nu}_{ij}) \prod_{m=1}^{M} \prod_{\langle i,j, \rangle} q_{ij}^z(Z_{ij}^m; \tilde{\gamma}_{ij}^m), \quad (4)$$

where $q_i^r(\cdot)$ and $q_{ij}^z(\cdot)$ are Bernoulli distributions parameterized by $\tilde{\alpha}_i$ and $\tilde{\gamma}_{ij}^m$, respectively. Conversely, $q_{ij}^c(\cdot)$ is a multinomial distribution with 9 states parameterized by $\tilde{\nu}_{ij}$; these states account for the 9 configurations of F_{ij} and $\bar{F}_{ij}$. Eq. (4) preserves the connection-wise dependencies and is tractable for large N.

We employ a coordinate descent algorithm to jointly optimize all unknown quantities. During the E-step, we fix Θ and iteratively update the elements of $Q(\cdot)$ to minimize the variational free energy. The updates for $\tilde{\nu}_{ij}$ and $\tilde{\gamma}_{ij}^m$ can be expressed in closed form given the other variational parameters. However, the updates for $\{\tilde{\alpha}_i\}$ are coupled. Therefore, we perform an inner fixed-point iteration until the region posterior converges. In the M-step, we fix $Q(R, F, \bar{F}, Z)$ and optimize the model parameters Θ. The prior and likelihood updates for $\{\pi^r, \pi^f, \mu, \sigma^2\}$ parallel those of a Gaussian mixture model. We then jointly optimize the edge density η and the latent noise ϵ via Newton's method.

Model Evaluation: The marginal posterior $q_i^r(R_i; \tilde{\alpha}_i)$ informs us about the disease foci. We evaluate the robustness of these region assignments via bootstrapping. Specifically, we fit the model to random subsets of the data while preserving the ratio of patients to neurotypical controls. We run two experiments, corresponding to subsets with 90% and 50% of the overall cohort, respectively. Our results are averaged across 100 data re-samplings.

Our canonical network corresponds to the idealized graph of functional differences: $F_{ij} \neq \bar{F}_{ij}$. Despite the confounding latent noise, governed by the parameter ϵ, we can approximate the canonical network based on the max *a posteriori* (MAP) solution for $\{R, F, \bar{F}\}$ and the parameter estimates $\hat{\Theta}$.

Finally, we perform a qualitative comparison of our proposed model with the Bayesian formulation in [6], which assume a homogeneous patient group, and with univariate t-tests on the pairwise rsfMRI correlation coefficients.

Synthetic Experiments: We have run simulations on synthetic data sampled from our model to demonstrate that our variational algorithm can recover the ground truth region labels. Fig. 2 illustrates the error in region assignments with respect to two quantities: the latent noise ϵ and the Gaussian separation $\Delta\mu/\sigma$ between adjacent connectivity states assuming equal variances.

In the first experiment (left), we sample disease foci based on the region prior π^r estimated from our autism dataset (see Table 1) and sweep both noise

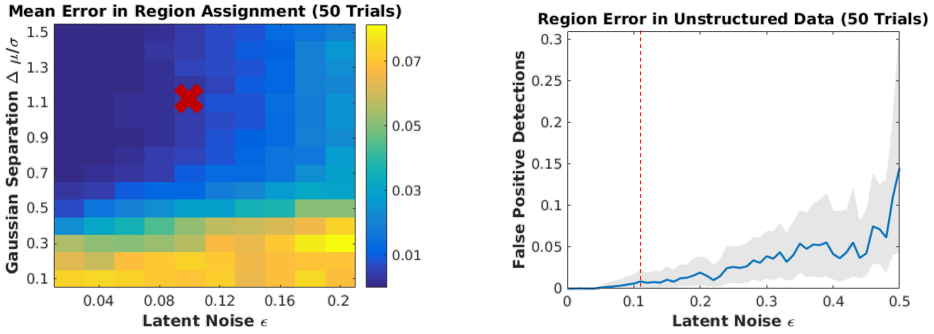

Fig. 2. Probability of error in the inferred region labels, as averaged across 50 generations of synthetic data. The red **X** and red line correspond to the noise regime estimated from our real-world dataset. **Left:** Disease foci were sampled according to π^r in Table 1. **Right**: Uniformly distributed changes in latent functional connectivity. Gray interval corresponds to the upper and lower standard deviation.

quantities. In the second experiment (right), we assume that the latent functional differences are uniformly distributed across the brain (i.e., $\pi^r = 0$) and compute the false positive assignments of regions as disease foci. Here, we have fixed the Gaussian separation according to our rsfMRI dataset and focus on the latent noise ϵ. The number of regions, cohort sizes and edge density η are fixed according to the values from our autism dataset. As seen, our algorithm performance is near-perfect for small values of ϵ and larger Gaussian separations. Encouragingly, the region assignment error is small in the noise regime of our real-world dataset, as marked with a red **X** (left) and a red line (right) in Fig. 2.

3 Population Study of Autism

We demonstrate our method on a cohort of 66 children with high-functioning ASD and 66 neurotypical controls, who were matched on the basis of age, gender and IQ. RsfMRI scans were acquired on a Phillips 3T Achieva scanner using a single-shot, partially parallel gradient-recalled EPI sequence (TR/TE = 2500/30 ms, flip angle = 70°, $res = 3.05 \times 3.15 \times 3$mm, 128 or 156 time samples). Children were instructed to relax and focus on a cross-hair while remaining still.

RsfMRI preprocessing includes slice time correction, rigid body realignment, and normalization to the EPI version of the MNI template using SPM [9]. The time series were temporally detrended, and we use CompCorr to estimate and remove spatially coherent noise from the white matter and ventricles, along with linearly detrended versions of the six rigid body realignment parameters and their first derivatives [10]. The cleaned data was spatially smoothed ($6mm$ FWHM Gaussian kernel), temporally filtered using a $0.01 - 0.1$ Hz pass band, and spike-corrected via tools from the AFNI package [11].

We define 116 cortical, subcortical and cerebellar regions based on the Automatic Anatomical Labeling (AAL) atlas [12]. The rsfMRI measure B_{ij}^l is com-

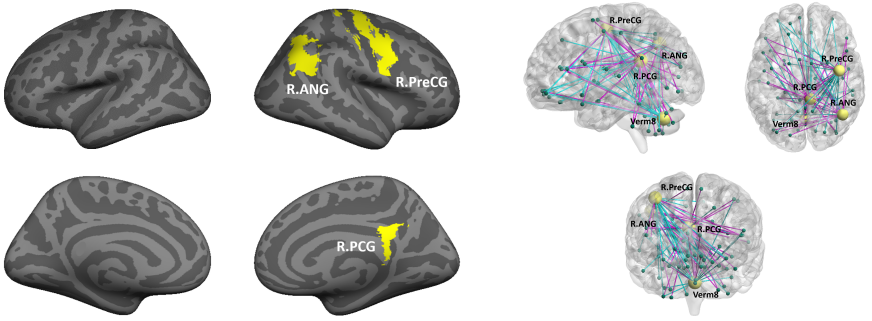

Fig. 3. Results of our heterogeneous patient model. **Left:** Disease foci projected onto the inflated cortical surface. **Right:** Canonical network of abnormal functional connectivity. Yellow nodes correspond to the disease foci. Blue lines signify reduced functional connectivity in ASD; magenta lines denote increased functional connectivity in ASD.

puted as the Pearson correlation coefficient between the mean time courses of regions i and j. We focus on deviations from baseline by centering the correlation histogram for each subject and fixing $\mu_1 = 0$. Our severity measures β_m correspond to the Autism Diagnostic Observation Schedule (ADOS) total raw score, normalized by the maximum possible test score.

Canonical Network Results: Fig. 3 illustrates the canonical network inferred by our model. The yellow nodes correspond to the disease foci, and we display connections that are consistently implicated across bootstrapping trials. Magenta and blue lines denote increased and reduced latent connectivity in ASD, relative to the neurotypical population. As seen, we identify four disease foci: the right precentral gyrus (R.PreCG), the right posterior cingulate gyrus (R.PCG), the right angular gyrus (R.ANG) and vermis 8 of the cerebellum (Verm8).

Our results are closely aligned with growing evidence, which suggests that brain abnormalities associated with ASD occur at the level of interconnected systems/modules [13, 14]. RsfMRI studies in neurotypical subjects have identified several intrinsically connected modules related to visual, motor, auditory, behavioral control, and interoceptive processes [15]. The nodes in Fig. 3 belong to two of these modules: the right precentral gyrus (R.PreCG) and the cerebellar vermis (Verm8) represent critical foci of the sensorimotor network that is specialized in the production of action, while the right posterior cingulate gyrus (R.PCG)

Table 1. Estimated model parameters for the proposed patient-specific model (top) and the homogeneous model of [6] (bottom).

	π^r	π_0^f	π_1^f	π_2^f	η	ϵ	μ_0	μ_1	μ_2	σ_0^2	σ_1^2	σ_2^2
Prop.	0.035	0.28	0.49	0.22	0.16	0.11	-0.18	0.00	0.23	0.037	0.031	0.030
Homogen.	0.0087	0.29	0.48	0.22	0.16	0.052	-0.18	0.00	0.22	0.037	0.032	0.031

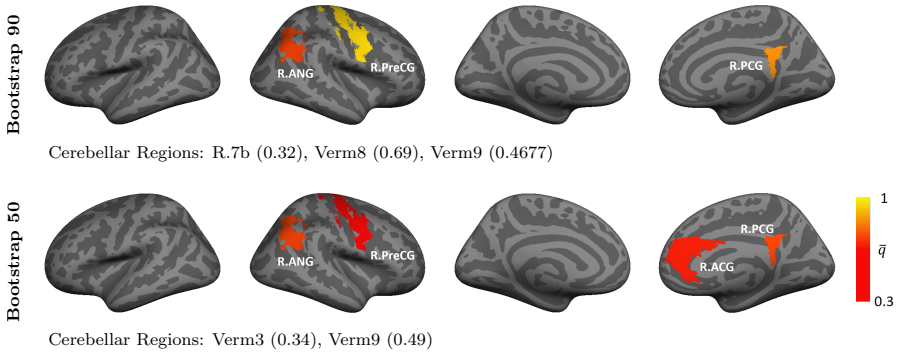

Fig. 4. Average marginal posterior probability $q_i^r(\cdot)$ for each community across 100 random samplings of the rsfMRI dataset. Top row includes 90% of the subjects in each subset, and the bottom row includes 50%. Reproducibility of cerebellar regions are listed underneath. The colorbar denotes the average posterior probability $\bar{q}_i^r$.

and the right angular gyrus (R.ANG) are both key nodes of the default mode network (DMN), which is more engaged during self-referential processing and social cognition [16]. Extant ASD research has largely focused on understanding social-communicative deficits in ASD and the potential involvement of the DMN. However, an emerging consensus suggests that movement abnormalities are also specific for ASD [17] and potentially rooted in the intrinsic functional organization of the brain [18]. For example, action execution, imitation, and emulation can be linked to shared functional dynamics between the sensorimotor and DMN systems [19]. As such, communication disruptions between these systems may negatively impact the development of internal action models, which are crucial to both sensorimotor and social skill development in children with ASD [20]. Considered together, our findings support the theory that motor behavior and self-referential processing deficits experienced by individuals with ASD can be jointly attributed to faulty connections within the brain.

Fig 4 reports the average posterior probability $\bar{q}_i^r(\cdot)$ of each region across 100 bootstrapped trials. We display only the regions for which $\bar{q}_i^r > 0.3$ to emphasize the most prominent patterns. As seen, our model consistently recovers the canonical network foci in Fig 3 when trained on 90% of the data. Remarkably, we are still able to detect the original network foci using half the dataset, which further validates the reproducibility of our Bayesian model. Finally, our bootstrapping experiments also implicate cerebellar regions adjacent to Vermis 8, which ties into broader theories of altered cerebellar functioning in ASD [21].

Fig. 5 compares our canonical network (left) with the model of [6] (middle), which assumes a homogeneous patient group, and with standard univariate tests (right). Notice that while the estimated model parameters in Table 1 are nearly identical, the proposed and homogeneous Bayesian models implicate different functional networks. Specifically, the homogeneous model identifies a single disease foci (R.ANG). However, incorporating the severity scores β_m seems

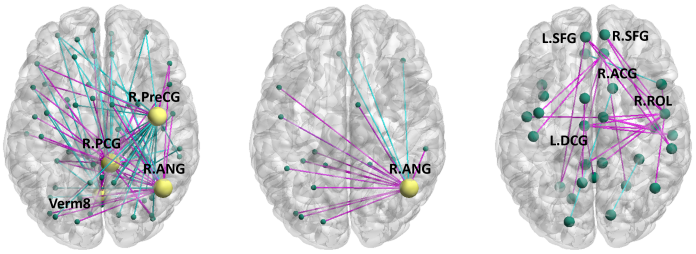

Proposed Method Homogeneous Connection T-Test

Fig. 5. Qualitative comparison of our proposed model of patient heterogeneity (left), the original Bayesian model described in [6] (middle), and the top connections ($p < 0.001$ uncorrected) via two-sample t-tests on the pairwise correlation values (right).

to provide an additional level of flexibility, which allows us to find robust effects in other brain regions. The connections implicated by two-sample t-tests form a markedly different pattern than the network model results; they tend to concentrate in the frontal cortex and anterior cingulate gyrus. This observation suggests that our disease foci provide a unique perspective of the data.

4 Conclusion

We have introduced a novel probabilistic framework that identifies group differences in functional connectivity while accommodating a heterogeneous clinical presentation. Specifically, we assume a latent graph organization that captures population-level effects. The influence of this latent structure on the data is moderated by the observed clinical severity scores for each patient. Synthetic experiments confirm that our variational algorithm can accurately infer ground-truth region labels under noise levels commiserate to real-world data. We further evaluate our model on a population study of high-functioning ASD. Our results implicated a distributed network of abnormal connectivity that concentrates in the precentral gyrus, posterior cingulate, angular gyrus and cerebellar vermis. We use bootstrapping to verify the robustness of our region assignments, and we demonstrate that our model identifies a richer set of functional differences than two baseline approaches, which do not account for patient heterogeneity.

Acknowledgments: This work was supported in part by the National Institute of Mental Health (R01 MH085328-09, R01 MH078160-07, and K01 MH109766), the National Institute of Neurological Disorders and Stroke (R01 NS048527-08), and the Autism Speaks foundation.

References

1. Fox, M.D., Raichle, M.E.: Spontaneous fluctuations in brain activity observed with functional magnetic resonance imaging. Nature **8** (2007) 700–711

2. Di Martino, A., Yan, C.G., Li, Q., Denio, E., Castellanos, F., et al.: The autism brain imaging data exchange: Towards a large-scale evaluation of the intrinsic brain architecture in autism. Molecular Psychiatry **19** (2014) 659–667
3. Meunier, D., et al.: Hierarchical modularity in human brain functional networks. Frontiers in Neuroinformatics **3** (2009) 37
4. Sporns, O., Zwi, J.: The small world of the cerebral cortex. Neuroinformatics **2** (2004) 145–162
5. Horga, G., Kaur, T., Peterson, B.: Annual research review: Current limitations and future directions in MRI studies of child- and adult-onset developmental psychopathologies? Journal of Child Psychology and Psychiatry **55** (2014) 659–680
6. Venkataraman, A., et al.: From brain connectivity models to region labels: Identifying foci of a neurological disorder. IEEE TMI **32** (2013) 2078–2098
7. Padmanabhana, A., et al.: The default mode network in autism. Biological Psychiatry: Cognitive Neuroscience and Neuroimaging **ePub** (2017) 1–11
8. Jordan, M., Ghahramani, Z., Jaakkola, T.S., Saul, L.K.: An introduction to variational methods for graphical models. Machine Learning **37** (1999) 183–233
9. Friston, K., et al., eds.: Statistical Parametric Mapping: The Analysis of Functional Brain Images. Academic Press (2007)
10. Behzadi, Y., et al.: A component based noise correction method (compcor) for bold and perfusion based fMRI. NeuroImage **37** (2007) 90–101
11. Cox, R.W.: Afni: Software for analysis and visualization of functional magnetic resonance neuroimages. Comp and Biomed Res **29**(3) (1996) 162 – 173
12. Tzourio-Mazoyer, N., et al.: Automated anatomical labeling of activations in SPM using a macroscopic anatomical parcellation of the MNI MRI single-subject brain. NeuroImage **15** (2002) 273–289
13. Schipul, S., Keller, T., Just, M.: Inter-regional brain communication and its disturbance in autism. Frontiers in Systems Neuroscience **5** (2011) 10
14. Vasa, R., Mostofsky, S., Ewen, J.: The disrupted connectivity hypothesis of autism spectrum disorders: Time for the next phase in research. Biological Psychiatry: Cognitive Neuroscience and Neuroimaging **1** (2016) 245–252
15. Damoiseaux, J., et al.: Consistent resting-state networks across healthy subjects. PNAS **103** (2006) 13848–13853
16. Mars, R., et al.: On the relationship between the "default mode network" and the "social brain". Frontiers in Human Neuroscience **6** (2012) 189
17. Ament, K., et al.: Evidence for specificity of motor impairments in catching and balance in children with autism. J Autism and Dev Disorders **45** (2015) 742–751
18. Nebel, M., et al.: Disruption of functional organization within the primary motor cortex in children with autism. HBM **35** (2014) 567–580
19. Bardi, L., et al.: Tpj-m1 interaction in the control of shared representations: New insights from tDCS and TMS combined. NeuroImage **146** (2017) 734–740
20. Mostofsky, S., Ewen, J.: Altered connectivity and action model formation in autism. Neuroscientist **17** (2011) 437–448
21. Becker, E., Stoodley, C.: Autism spectrum disorder and the cerebellum. Int Review Neurobiology **113** (2013) 1–34